Journal of The Electrochemical Society, **152** (4) A759-A766 (2005)
0013-4651/2005/152(4)/A759/8/$7.00 © The Electrochemical Society, Inc.

Simultaneous Measurements of Species and Current Distributions in a PEFC under Low-Humidity Operation

Xiao-Guang Yang,[a,*] Nick Burke,[a] Chao-Yang Wang,[a,*,z] Kazuya Tajiri,[b,c] and Kazuhiko Shinohara[b]

[a]*Electrochemical Engine Center, and Department of Mechanical and Nuclear Engineering, The Pennsylvania State University, University Park, Pennsylvania 16802, USA*
[b]*Nissan Motor Company Limited, Nissan Research Center, Kanagawa 237-8523 Japan*

An experimental technique has been developed to conduct simultaneous measurements of species concentration and current density distributions using a segmented cell of 50 cm^2. Twelve segmented subcells in conjunction with a multichannel potentiostat were employed to measure the current distribution, and two sets of multiposition microactuators and micro gas chromatographs were used to measure gas concentration distributions on the anode and cathode sides simultaneously. Distribution data are shown systematically for a polymer electrolyte fuel cell (PEFC) operated under low-humidity cathode conditions and at 80°C and 2 atm. The O_2 concentration profile for the PEFC is generally linear and can be well predicted by a simple mass balance analysis, the anode water concentration profile is closely tied to the net water transport rate through the membrane, and the net water transport coefficient ranges between 0.05 and 0.30 even under very dry cathode conditions, suggesting the presence of strong back-diffusion of water from the cathode to the anode despite rather dry cathode gas.
 [DOI: 10.1149/1.1864492]

Manuscript submitted July 18, 2004; revised manuscript received September 14, 2004. Available electronically March 7, 2005.

Low-humidity operation of polymer electrolyte fuel cells (PEFCs) is a current focus for automotive applications. In such an operation, membrane dehydration and electrode flooding by liquid water can coexist in a PEFC, thereby significantly compounding the fundamental phenomena governing the cell performance and operational stability. Detailed quantification of localized behaviors in this type of PEFC is highly desirable for a better understanding of cell performance and durability.

Various experimental techniques to measure the current distribution have been developed, including the printed circuit board approach by Brown *et al.*[1] and Cleghorn *et al.*,[2] the partial membrane electrode assembly (MEA)/subcell approach and passive current mapping technique by Stumper *et al.*,[3] the magnetic loop current sensor approach by Wiser *et al.*,[4] the segmented cell/resistor network approach by Noponen *et al.*[5] and Brett *et al.*,[6] and the segmented cell/multipotentiostat approach of Wang and co-workers.[7-9] In addition, localized ac impedance and current distribution have been measured on a segmented PEFC with a single linear channel at 30°C with 1 atm fully humidified H_2 and dry air inlets.[6] Mench *et al.*[9] demonstrated the first measurement of water, hydrogen, and oxygen concentration distributions using a micro gas chromatograph. A review of these prior efforts in detail was provided most recently by Wang.[10] A common problem prevailing in all prior work to date is the inability to produce a similar level of current density expected from a nonsegmented single cell under operating conditions characteristic of automotive applications. The problem largely originates from excessive contact resistances existing between many segment pieces and the gas diffusion layer (GDL).

The objective of the present work is twofold. One is to present an improved segmented cell technique that enables measurement of the current distribution that closely matches the performance expected from single cell testing. This improvement makes it possible to obtain distribution data representative of the physicochemical processes occurring in actual low-humidity PEFCs. The second objective is to demonstrate a capability to *simultaneously* measure the current and mass distributions at both electrodes in conditions relevant to the automobile application with a low-humidity air supply.

Experimental

The present test cell is an improved design of the cell fixture used in our previous work.[7] Among many design modifications to minimize voltage losses, 1/16 in. (~1.6 mm diam) silver wires instead of stainless steel wires were soldered to stainless steel rib segments for current and voltage measurements. We carefully aligned each rib, ensuring that various segments inside the cell are well under equipotential as stipulated by a multichannel potentiostat. On each side of the segmented cell, a 0.5 in. thick polycarbonate plate was used to electrically isolate the current collectors (ribs) and as a manifold to direct the gas flow. Twenty-four gold-plated stainless steel ribs (0.81 mm wide, 6.4 mm deep, and 56.6 mm long) were inserted into grooves (5.4 mm deep) machined in the polycarbonate plate, as shown in Fig. 1. The ribs, along with Teflon inserts and a sheet of gasket (1 mm thick), form a two-pass serpentine gas flow field. The formed flow field has a channel width and depth of 2.08 and 1.0 mm, respectively, and the landing width is 0.81 mm. The same segmented flow field plate was used for both anode and cathode. Ribs with their silver wires leading through the back of the polycarbonate plate were grouped into 12 electrically isolated subcells for external voltage and current measurements. In addition, 12 ports periodically located along both anode and cathode flow fields were used for gas-sampling, as shown in Fig. 1. In addition, two 0.5 in. thick stainless steel backing plates were used to physically support the polycarbonate plates. Electric cartridge heaters inserted into the holes on the sides of the backing plates were used to maintain the cell temperature. The current density and species distribution measurements can be conducted simultaneously in this instrumented cell.

Commercially available MEA (50 cm^2) and carbon paper as the GDL were used without segmentation. The membrane (EW < 1000) used was 18 μm thick, and the GDL was a Toray carbon paper TGPH-090 coated with a microporous layer. In all experiments, pure hydrogen and air were used as the anode and cathode gases. The flow stoichiometry for the anode and the cathode was ξ_a/ξ_c = 1.5/2.0 at 1 A/cm^2 (*i.e.*, constant flow rates equivalent of 1.5 and 2 A/cm^2). The cell temperature was set at 80°C, and the exit pressure was set at 2 atm (absolute), unless otherwise indicated. The dew point was at 80°C for the H_2 inlet [relative humidity (RH) = 100%] and 64°C or 49°C for the air inlet (*i.e.*, RH = 50% or 25% relative to 80°C). All test parameters can be computer controlled by a Fuel Cell Test System (Arbin Instruments, TX). To ensure consistent and reproducible data, all MEAs in this work were preconditioned at 0.7 V under full humidification at 80°C and ξ_a/ξ_c = 1.5/2.0 at 1 A/cm^2, and subsequently the cell stayed at a desired

* Electrochemical Society Active Member.
[c] Present address: Electrochemical Engine Center, and Department of Mechanical and Nuclear Engineering, The Pennsylvania State University, University Park, Pennsylvania 16802, USA.
[z] E-mail: cxw31@psu.edu

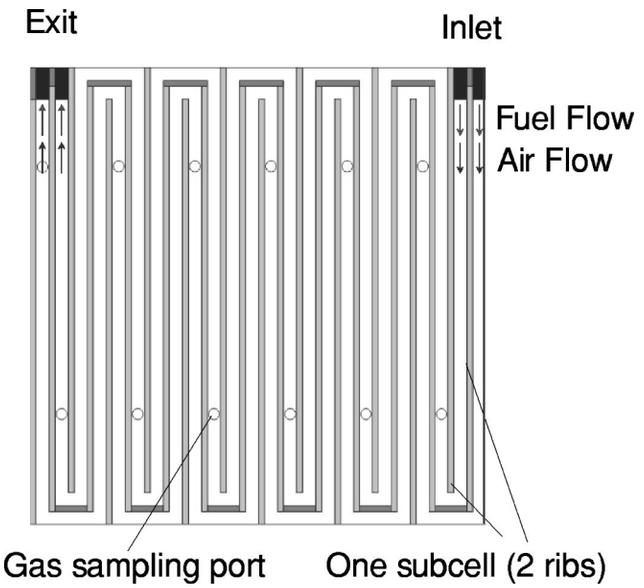

Figure 1. Schematic diagram of two-pass serpentine flow field and location of gas sampling ports; paired arrows for the anode and cathode indicate flow directions. Twenty-four current collecting ribs are inserted in grooves in polycarbonate plate. Each subcell consists of two ribs. Each gas channel contains six gas sampling ports.

humidification condition at least for 30 min before the data were taken.

Figure 2 displays a schematic diagram of the experimental setup capable of simultaneously measuring the species, current, and high-frequency impedance distributions in the instrumented cell. The 12 subcells were connected to a multichannel potentiostat for current distribution measurements under a specified cell voltage. Two Micro gas chromatographs (MicroGC) from Agilent were used to measure water, hydrogen/oxygen, and nitrogen along the flow paths of the anode/cathode, respectively. In each MicroGC two columns separate the gas species, a Plot-U column and a molecular sieve column with a backflush module to prevent excess water damage. On each side of the cell, 12 1/16 in. stainless steel tubes connected 12 gas sampling

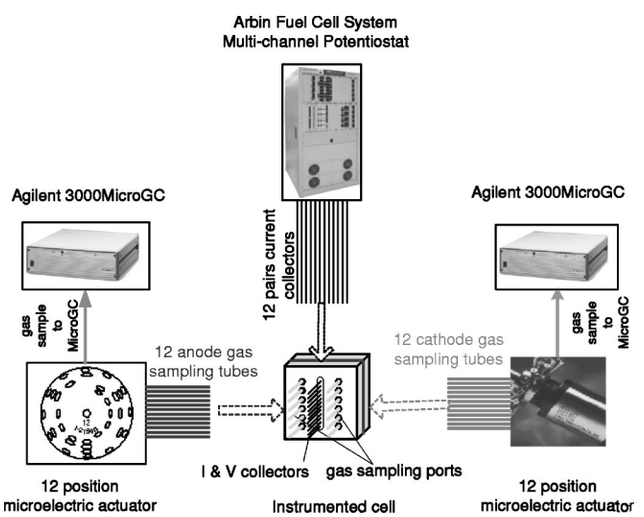

Figure 2. Schematic diagram of experimental setup for simultaneous measurements of anode/cathode species, current, and high-frequency resistance distributions in an operating cell.

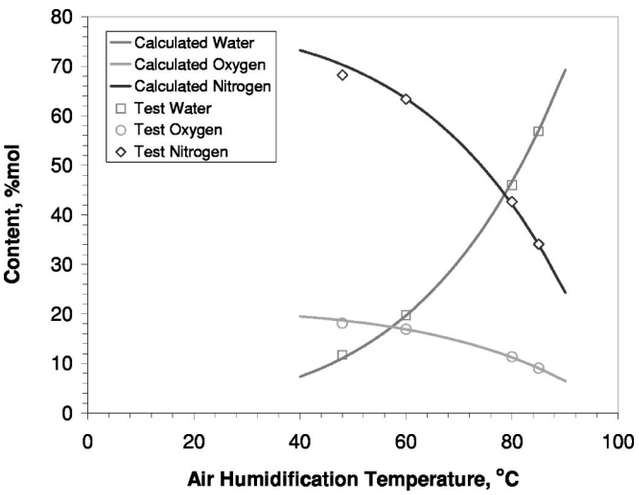

Figure 3. Calibration of MicroGC: the measured composition data are compared with theoretical values at various temperatures.

ports to 12 inlet ports in a multiport microelectric actuator (Valco), and only one exit port of the actuator was connected to the MicroGC. The actuator can automatically switch the connection from one of 12 sampling ports to the inlet of the MicroGC at one time. The amount of sampling gas taken by the MicroGC was very small (about 20 μL for each run). To prevent water condensation, all sampling tubes and the multiposition valve were heated above 100°C. The temperature of the inlet into the MicroGC was set at 120°C to prevent liquid water from entering the columns. The carrier gas used was helium for the Plot-U column for water measurement and argon for the molecular sieve column for the H_2, O_2, and N_2 measurements. The pressures of both carrier gases were set at 80 psig (1 atm = 14.7 psig) to ensure the accuracy and repeatability of the measurements. The MicroGC took ~3 min to complete a sample analysis. Three or more gas measurements were performed to ensure repeatability of MicoGC analysis results. Although the fuel cell reached steady state under each voltage within 15–30 min, it usually took an additional 2-3 h to complete mass measurements for all 12 channels at a specific voltage. Typical variations between different measurements under identical conditions were ±1.5% for O_2 and ±4% for H_2O, respectively.

Calibration of the MicroGCs was conducted with air fully humidified at 80°C using a high-precision saturator. Then, the calibrated parameters, including the retention times, responses, and preknown concentrations of components in a calibration gas, were provided to the MicroGC data processing software to specify conversions of peak areas into mole fractions (mol %). Once calibrated, the MicroGC was employed to measure compositions of air humidified at 49, 60, and 85°C. The calibration curves are shown in Fig. 3, demonstrating good agreement between the MicroGC-measured data and theoretical calculations.

Results and Discussion

A systematic set of experiments was carried out under the above-mentioned conditions for three cell voltages: 0.7, 0.6, and 0.5 V, and two cathode inlet RH:50% and 25%, while the anode inlet RH was always maintained at 100%. The anode and cathode were in co-flow.

Species distribution measurements.—Figures 4-6 show the measured mole fraction distributions of O_2 and H_2O in the cathode as well as H_2 and H_2O in the anode with 50% RH air inlet at 2 atm and under cell voltages of 0.7, 0.6, and 0.5 V, respectively. In addition to reactants and water, nitrogen was also sampled and analyzed by the MicroGC, but its data are not shown here. The three cell voltages

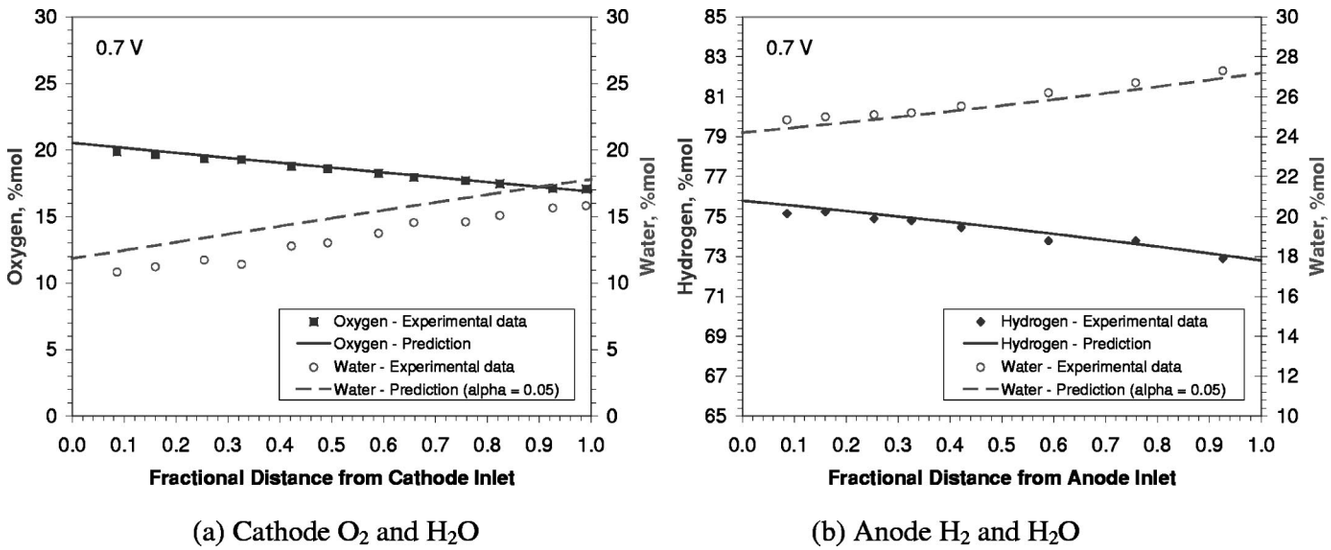

Figure 4. Measured (symbols) and calculated (lines) species distributions at 0.7 V and with anode and cathode inlet RH of 100 and 50%, respectively: (a) cathode O_2 and H_2O, and (b) anode H_2 and H_2O.

were chosen to represent three distinctive regimes of the polarization curve, the kinetic, ohmic, and mass-transport control regions.

Figure 4a shows the O_2 and H_2O mole fraction profiles along the cathode flow at a cell voltage of 0.7 V. The oxygen concentration decreases linearly from the inlet toward the exit, indicating approximately constant consumption rate or current density distribution. A constant flow rate equivalent to 2 A/cm^2 was used in the experiments, thus making the real stoichiometry under this high cell voltage or low current density ($\sim$0.5 A/cm^2 as seen from Fig. 10) close to 4. Therefore, one can expect the oxygen concentration to vary much more if under a true stoichiometry of 2.

The water mole fraction displayed in Fig. 4a increases linearly as well, reaching 15.8 mol% at the exit. This level of water concentration is still lower than the saturated water vapor mole fraction ($\sim$23.5 mol% in 2 atm). A water balance calculation for the cathode gas indicates that all of the product water from the oxygen reduction reaction (ORR) is removed by the cathode exhaust under this dry cathode operating condition. Figure 4b shows that the H_2 concentration slightly decreases from 75.2 mol% near the inlet to 73.0 mol% at the exit along the anode flow field, due to the hydrogen oxidation reaction (HOR). Correspondingly, the water concentration in the anode binary gas increases from full humidification to slight overhumidification. Water condensation thus likely occurs in regions close to the anode exit, resulting from the consumption of H_2. The lines shown in Fig. 4a and b correspond to mass balance calculations, to be discussed in the next subsection.

Figure 5 shows similar mole fraction profiles at 0.6 V. The oxygen concentration decreases at a slightly larger slope than the 0.7 V case. Water uptake in the cathode gas also increases at a greater rate, reaching $\sim$20 mol% at the exit; this value is close to the saturation level. On the anode side, Fig. 5b interestingly indicates that the water and hydrogen concentrations remain nearly constant along the gas channel at this cell voltage. This implies that water loss from the anode to the cathode by electro-osmotic

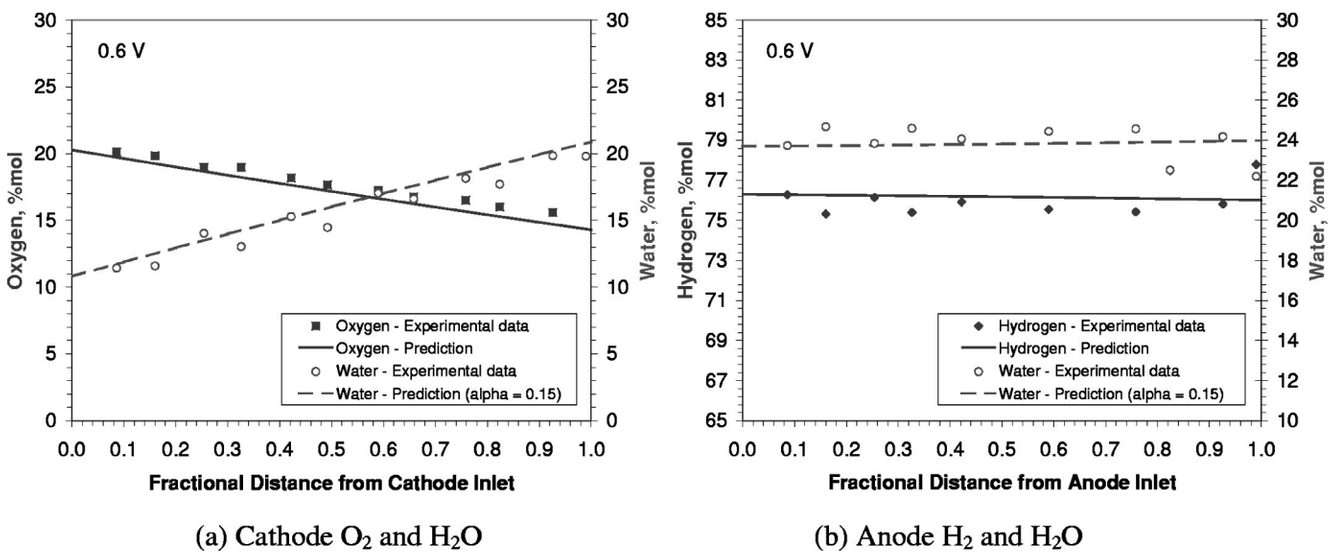

Figure 5. Measured (symbols) and calculated (lines) species distributions at 0.6 V and with anode and cathode inlet RH of 100 and 50%, respectively: (a) cathode O_2 and H_2O, and (b) anode H_2 and H_2O.

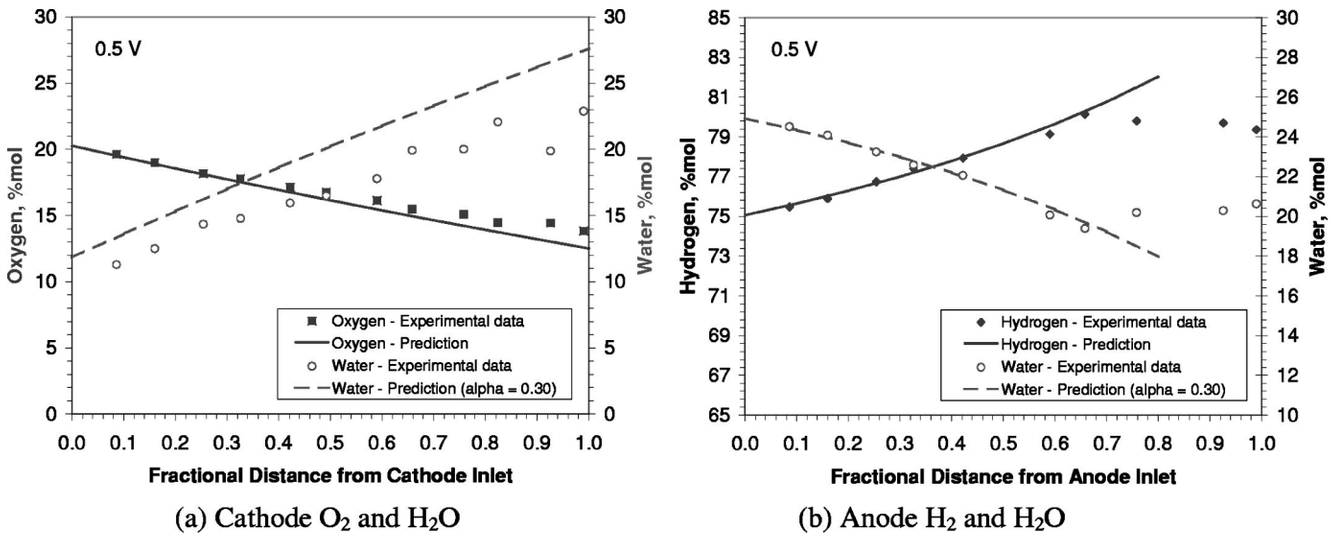

Figure 6. Measured (symbols) and calculated (lines) species distributions at 0.5 V and with anode and cathode inlet RH of 100 and 50%, respectively: (a) cathode O_2 and H_2O, and (b) anode H_2 and H_2O.

drag and forward diffusion (as the anode RH is equal to 100% but the cathode RH is lower throughout the cell) as compared to the hydrogen consumption by HOR is equal to the molar ratio of H_2O to H_2 at the inlet, $\sim 1/3$ in this case. It follows that 2α should be closely equal to 1/3, or $\alpha \approx 1/6$. The ability to maintain uniform distribution of the reactant and water vapor at full humidification under this special situation may be of technological and fundamental interest.

Figure 6 shows the species measurements at 0.5 V along the cathode and anode flows, respectively, under otherwise the same conditions as in Fig. 4 and 5. The O_2 concentration still tends to decrease linearly toward the exit. However, water uptake in the cathode gas begins to reach the saturation level near the exit. Note that the two data points of the water concentration closest to the exit exhibit some scattering, suggesting that there is likely condensation and two-phase formation in this part of the fuel cell. The H_2 and H_2O concentration profiles in the anode, as displayed in Fig. 6b, illustrate an interesting new pattern at 0.5 V. The H_2 mole fraction increases and the H_2O mole fraction decreases along the first two-thirds of the fuel cell. This is experimental evidence of electro-osmotic drag dominating the water transport through the membrane. At this cell voltage, the average current density reaches ~ 0.8 A/cm^2 (shown in Fig. 10), and consequently the enhanced electro-osmotic drag makes the anode lose water at a greater rate than H_2 consumption. Hence, the water mole fraction decreases and the H_2 mole fraction increases. Toward the exit of the fuel cell, the water concentration on the cathode becomes larger than that in the anode, thereby causing back-diffusion of water to offset the electro-osmotic drag. Also, in this region, the local current density becomes small primarily due to the oxygen depletion effect on the cathode, thus weakening the electro-osmotic water flux. The end result is that the water concentration in the anode begins to increase at the dimensionless distance of 65% from the anode inlet, signifying the anode gain in water.

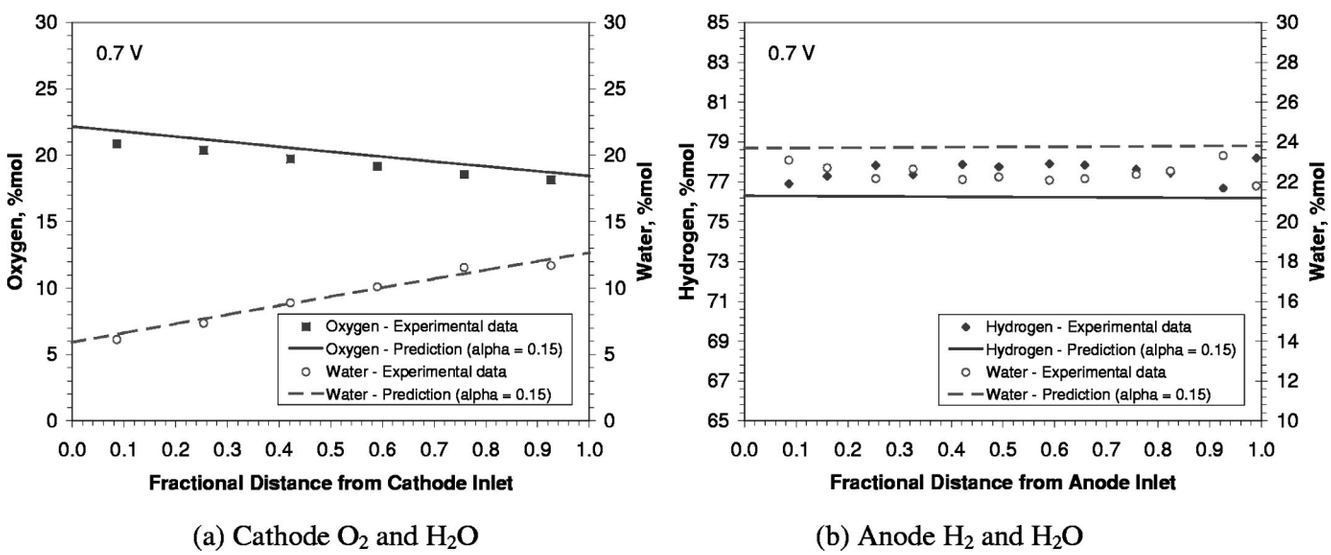

Figure 7. Measured (symbols) and calculated (lines) species distributions at 0.7 V and with anode and cathode inlet RH of 100 and 25%, respectively: (a) cathode O_2 and H_2O, and (b) anode H_2 and H_2O.

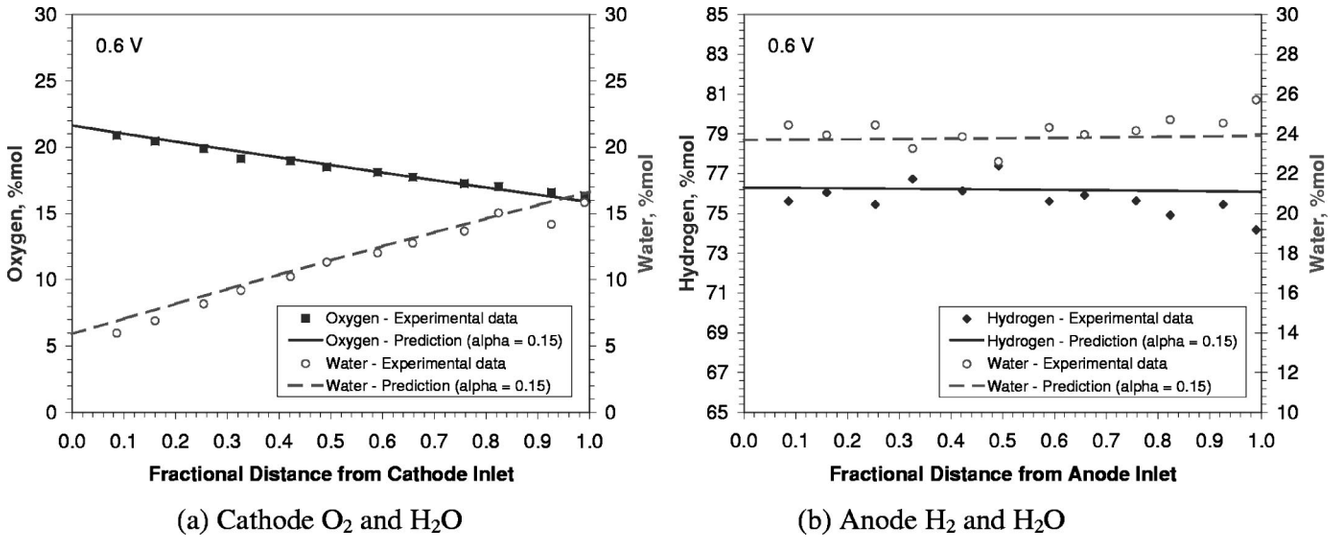

Figure 8. Measured (symbols) and calculated (lines) species distributions at 0.6 V and with anode and cathode inlet RH of 100 and 25%, respectively: (a) cathode O_2 and H_2O, and (b) anode H_2 and H_2O.

Figures 7-9 show similar measurements of anode and cathode species under a drier air inlet (RH = 25%) for the same three cell voltages of 0.7, 0.6, and 0.5 V, respectively. Due to the drier cathode, the anode is expected to lose more water under stronger forward diffusion in this condition. Although Fig. 7a displays normal linear profiles of cathode O_2 and H_2O, Fig. 7b indicates a nearly uniform distribution of both H_2 and H_2O in the anode. This behavior is contrasted to that of Fig. 4b for cathode inlet RH 50% and suggests that the anode water loss occurs at a rate comparable to H_2 consumption already at 0.7 V if the forward diffusion is strengthened.

Figure 8 displays the reactant and water concentration distributions in both cathode and anode at 0.6 V. The anode gas still maintains nearly constant compositions along the flow field. With a further decrease in cell voltage (or an increase in the average current density), Fig. 9 shows the species distribution data in cathode and anode at 0.5 V. Figure 9a shows that at this voltage or at a current density level of ~ 0.75 A/cm^2, the cathode gas remains in the low-humidity operation throughout the cell, with a water mole fraction at the exit under 19 mol%. The anode water concentration profile displayed in Fig. 9b demonstrates the same decrease-increase pattern as in Fig. 6b for the same reason explained earlier. Note that the minimum point of water concentration in the anode, which typically signifies a transition in dominance of membrane water transport from the electro-osmotic drag to back-diffusion, occurs around the dimensionless distance of 70% from the anode inlet. At this location, the anode water mole fraction reads $\sim 19\%$ (Fig. 9b), whereas the cathode water in the gas channel is only 15% (Fig. 9a). This seems to suggest forward-diffusion from the anode to the cathode, rather than back-diffusion. However, water diffusion through the polymer membrane is driven by the water concentration gradient between the anode and cathode sides of the membrane. It is expected that the cathode water concentration in the vicinity of the membrane is well above that in the gas channel due to ORR water production locally.

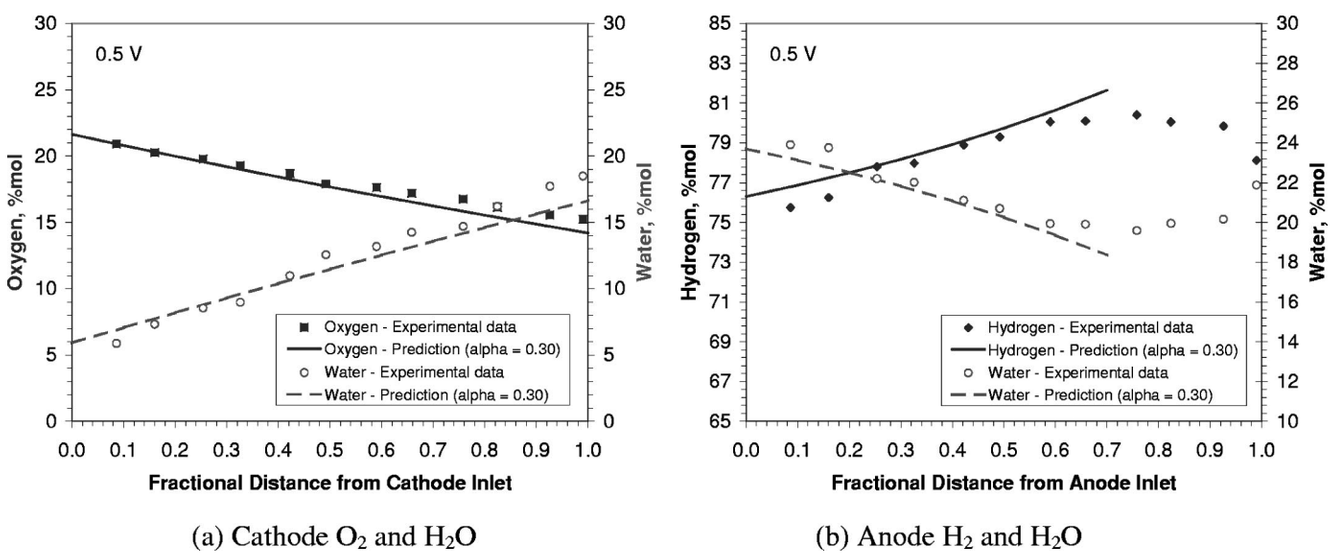

Figure 9. Measured (symbols) and calculated (lines) species distributions at 0.5 V and with anode and cathode inlet RH of 100 and 25%, respectively: (a) cathode O_2 and H_2O, and (b) anode H_2 and H_2O.

Therefore, back-diffusion prevails and results in the decrease-increase shape of the anode water concentration profile.

Mass balance calculations.—To further explore the measured species concentration profiles, we performed mass balance calculations under steady state and a constant current density assumption. The assumption of constant current density can be justified somewhat by the relatively constant current distribution data to be shown shortly, as well as by the nearly linear characteristics in O_2 concentration profiles under all experimental conditions considered in this work. Further, we assume that H_2 and O_2 crossover through the membrane is negligibly small. The H_2 crossover current ranged typically between 2 and 4 mA/cm^2 through the Gore PRIMEA® 56 Series MEA under 70°C and ambient pressure,[11] and was 3.3 mA/cm^2 for Nafion 112 MEA under H_2/O_2 (270 kPa) and 80°C.[12] This level of H_2 crossover flux can be safely neglected from the present calculations for current densities greater than 300 mA/cm^2 and fall well within the experimental errors of species measurements. Similarly, the O_2 permeability through the membrane was reported to be half that of H_2,[13] thus O_2 crossover can be ignored for the analysis of species concentrations in the cathode.

The water molar rate (mol/s) at the location x/L along the cathode flow can be expressed as

$$n_{w,x,c} = n_{w,in,c} + n_{w,R,x} + n_{w,T,x} \quad [1]$$

where $n_{w,in,c}$ is the water molar flow rate at the cathode inlet, $n_{w,R,x}$ is the production rate over the length from 0 to x, *i.e.*, it equals IA/2F x/L, and $n_{w,T,x}$ is the net flux of water transport through the membrane from the anode to cathode, *i.e.*, αIA/F x/L. The parameter α is the net water transport coefficient through the membrane defined as the ratio of the net water flux to the protonic flux, thus the unit is the number of H_2O/H^+. This parameter is a combined result of the electro-osmotic drag and molecular diffusion of water through the membrane.

Similarly, the O_2 molar flow rate (mol/s) at the location x/L can be written as

$$n_{O_2,x} = n_{O_2,in} - n_{O_2,R,x} \quad [2]$$

The mole fractions of H_2O and O_2 at the location x/L in the cathode flow are thus derived to be

$$X_{w,c,x} = \frac{\dfrac{\xi_c I_{ref}}{0.21}\dfrac{P_{sat}RH_c}{P - P_{sat}RH_c} + \dfrac{Ix}{L}(2 + 4\alpha)}{\dfrac{\xi_c I_{ref}}{0.21}\dfrac{P}{P - P_{sat}RH_c} + \dfrac{Ix}{L}(1 + 4\alpha)} \quad [3]$$

and

$$X_{O_2,c,x} = \frac{\xi_c I_{ref} - \dfrac{Ix}{L}}{\dfrac{\xi_c I_{ref}}{0.21}\dfrac{P}{P - P_{sat}RH_c} + \dfrac{Ix}{L}(1 + 4\alpha)} \quad [4]$$

where ξ_c is the cathode stoichiometry set at 2.0 in this study, I_{ref} is the reference current density, 1 A/cm^2, P_{sat} is the saturated water vapor pressure at the cell temperature, RH_c is the relative humidity of the cathode inlet, and P is the cell pressure.

Similarly for the anode side, the hydrogen and water fluxes at the location x/L can be calculated, respectively, by

$$n_{H_2,x} = n_{H_2,in} - n_{H_2,R,x} \quad [5]$$

and

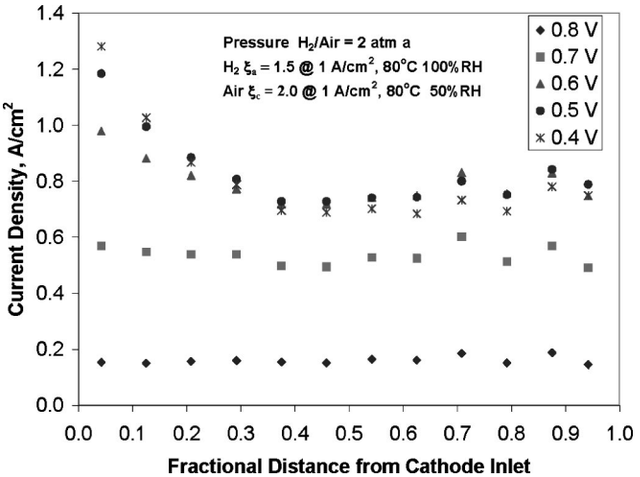

Figure 10. Local current density profiles for 50% RH cathode inlet.

$$n_{w,x,a} = n_{w,in,a} - n_{w,T,x} \quad [6]$$

This yields the following expression for the H_2 mole fraction in the fuel stream at the location x/L

$$X_{H_2,x} = \frac{\xi_a I_{ref} - \dfrac{Ix}{L}}{\dfrac{\xi_a I_{ref} P}{P - P_{sat}RH_a} - \dfrac{Ix}{L}(1 + 2\alpha)} \quad [7]$$

and it follows that the anode H_2O mole fraction is given by

$$X_{w,a,x} = 1 - X_{H_2,x} \quad [8]$$

Comparisons between experiments and calculations.—To use Eq. 3, 4, 7, and 8, we assume a value for α and use the measured average current density (from Fig. 10 and 11) in each case. Because α is a combined result of electrochemical drag and diffusion in the membrane, it varies with the operating conditions. Here we use α as the only fitting parameter to obtain calculations for all the experi-

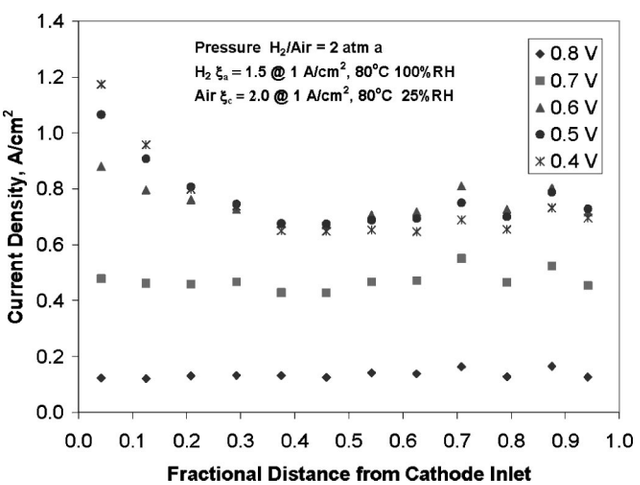

Figure 11. Localized performance along fractional distance from cathode inlet with 25% RH air inlet.

ments reported in this work. These calculations are represented as lines in Fig. 4-9 with the respective α-values indicated.

Generally, the agreement between calculations and measurements of O_2 concentration is very good in all cases. This suggests that the O_2 profile in the cathode is less dependent on the water transport characteristics inside the cell as long as the average current density can be accurately obtained. However, the H_2O concentration profiles along the anode and cathode strongly depend on multimodal water transport through the membrane in addition to ORR water production. For the 50% RH air inlet (Fig. 4-6), the best-fitted values of α were equal to 0.05, 0.15, and 0.30 H_2O/H^+ for the cell voltages of 0.7, 0.6, and 0.5 V, respectively. Using these constant α-values, reasonable agreement between the experimental data and mass balance calculations is possible as shown in Fig. 4-6. Further, the general trend of increasing α with the decrease in cell voltage (or increase in the current density) is physically reasonable and suggests the dominant role of electro-osmotic drag in water transport through the membrane in the present study of low-humidity operation.

The special case where the water and hydrogen concentrations remain constant along the anode channel can be examined in more detail using Eq. 7; that is

$$X_{H_2,x} = \frac{\xi_a I_{ref} - \frac{Ix}{L}}{\frac{\xi_a I_{ref} P}{P - P_{sat} RH_a} - \frac{Ix}{L}(1 + 2\alpha)} = \frac{P - P_{sat} RH_a}{P} \qquad [9]$$

It thus follows that

$$\alpha = \frac{P_{sat} RH_a}{2(P - P_{sat} RH_a)} \qquad [10]$$

This condition, Eq. 10, ensures that water and hydrogen concentrations in the anode are constant throughout.

Values of the net water transport coefficient estimated from the present study are much lower than the pure electro-osmotic drag coefficient of water that was typically reported somewhere between 1 and 2.5 H_2O/H^+,[14-16] with unity for underhydrated membranes and 2.5 for membranes equilibrated with liquid water. This implies a strong role of back-diffusion due largely to the thin membrane (18 μm) used and perhaps also to the presence of a microporous layer adjacent to the catalyst layer. The back-diffusion of water through the membrane could be established by the local buildup of water concentration within the cathode catalyst layer in the vicinity of the membrane, even though the cathode gas channel is largely undersaturated. Use of the microporous layer as done here promotes this local buildup of water and minimizes the membrane from being dehydrated by the very dry gas. Janssen and Overvelde[17] also analyzed the water transport through different MEAs (N105 and N112) by collecting water in the exhaust streams using cold traps. They reported a net water transport coefficient of 0.05-0.08 H_2O/H^+ with fully humidified anode and dry cathode inlets at current densities of 0.4 and 0.6 A/cm^2, 60°C and 1.5 or 3.0 atm, and a negative value from −0.3 to −0.05 for dry anode and humidified or dry air inlets under otherwise the same conditions. Our α-data appear to be consistent with the finding of Janssen and Overvelde.[17]

Figures 7-9 show that the experimental species concentration profiles can be reasonably matched with α equal to 0.15, 0.15, and 0.30 for the cell voltages of 0.7, 0.6, and 0.5 V with 25% RH of the cathode inlet. As compared to the more wet cathode 50% RH (*i.e.*, at the inlet), the only change in α-value is at 0.7 V, where a larger α (0.15 *vs.* 0.05) is fitted for the drier cathode inlet (25% RH). This is expected as the forward diffusion promoted by the lower water concentration in the cathode gas channel aids in electro-osmotic drag. However, the unchanged α-values at 0.6 and 0.5 V imply that the water transport characteristics through thin membranes are insensitive to the cathode inlet RH.

Finally, a monotonic water concentration profile in the anode always results as long as a constant α is employed. This is why the mass balance model using constant α as presented above cannot capture the decrease-then-increase pattern in the anode water concentration, as shown in Fig. 6b and 9b. To simulate these complex profiles, one must use a variable α that changes from a positive value to a negative value at the point of minimum water mole fraction in the anode. Such a change in the sign of α physically implies the transition in dominance of water transport by electro-osmotic drag to back-diffusion. Figures 6b and 9b also demonstrate the need for a sufficient RH level at the anode inlet for the anode side of the membrane not to dry out.

Current distribution measurements.—Figures 10 and 11 show the current density distributions measured simultaneously in the same experiments of species measurements for the cathode inlet RH of 50 and 25%, respectively, and under a range of cell voltages. Overall, the cell performance is better with the 50% RH cathode inlet than the one with 25% RH. For example, the average current density at 0.7 V in the more humidified cathode is 0.534 A/cm^2, as compared to 0.471 A/cm^2 for the 25% RH cathode inlet. Under each cathode RH condition, it is also observed that the local current density is generally uniform for cell voltages higher than 0.7 V. This is because the true stoichiometry is as high as 4 under the correspondingly low current densities such that the O_2 depletion effect is insignificant. Also, the increase in the water concentration from the cathode inlet to the outlet is small due to the large stoichiometric flow; consequently, the ohmic loss in the ionomer stays roughly similar.

However, at cell voltages lower than 0.6 V, we see consistent current density profiles in both Figures 10 and 11, being higher in the first one-third portion of the fuel cell and becoming approximately uniform in the last two-thirds of the fuel cell. We believe that in the region close to the inlet, the membrane is fully hydrated and the water concentration inside the catalyst layer is beyond the saturation level as a result of high current density or water production rate, even though the GDL is exposed to very dry gas in the channels. Higher proton conductivity in the ionomer and higher O_2 concentration then combine to yield higher current density locally. Note that such a current density profile in the low-humidity cell results from the fact that the membrane was kept wet initially in the present work. The possibility of oversaturation and even flooding inside the electrode even when the outer surface of GDL is exposed to dry air (50% and 25% RH) seems to be verifiable by rapid-scan potentiostatic polarization tests. Instead of holding each voltage point at steady state, one can scan the polarization curve from open circuit to 0.4 V at a rate of 10 mV/s (the whole process takes only 55 s). Thus, the rapid-scan polarization can effectively suppress the flooding effect (if there is any), which has a much longer time constant (of the order of 10 min). Our rapid-scan experiments (not shown here) indicate that the transient cell performance increases by ~30% as compared to the steady-state measurement under the same test conditions. This is strongly indicative of electrode flooding occurring in the cell. Moreover, the highest local current density in the transient measurements appears at the dimensionless distance of 30% from the inlet rather than immediately at the inlet as shown in steady-state tests. The highest local performance appearing in the middle of the flow field is characteristic of low-humidity cells when membrane hydration and oxygen depletion play equally important roles.

Conclusions

We have demonstrated an experimental technique capable of simultaneously measuring species and current distributions using an instrumented fuel cell of 50 cm^2. Extension of this technique to include the measurement of the high-frequency resistance distribution in the membrane is straightforward, provided that a multichannel ac impedance analyzer is available. Detailed experimental data under low-humidity cathode conditions were presented to show the

effectiveness of this detailed diagnostic technique in providing comprehensive insight into the fuel cell fundamentals. Specifically, the following conclusions can be drawn from this study.

1. The O_2 concentration profiles measured along the cathode flow field can be well predicted by a simple mass balance analysis, given the accurate information of the current density.

2. Three patterns of the water concentration profile in the anode were measured: (*i*) monotonically increasing due to faster H_2 consumption by HOR, (*ii*) staying uniform, and (*iii*) decreasing due to faster water transport from the anode to the cathode through the membrane and then increasing due to enhanced back-diffusion of water. The shape of the anode water concentration profile hinges upon the extent of water transport through the membrane.

3. The net water transport coefficient through the membrane, resulting from both electro-osmotic drag and diffusion, ranges between 0.05 and 0.30 in all cases considered. This value is much lower than the pure electro-osmotic drag coefficient in fluorinated membranes, indicating that there exists strong back-diffusion of water despite very dry cathode conditions. The values of net water transport coefficients also increase as the cell voltage decreases or the current density increases.

4. The current density distributions measured under both 25 and 50% RH cathode inlet conditions show highest local current density near the dry cathode inlet, thus suggesting that membrane dehydration in the inlet region is absent under these operating conditions. It is speculated that the carbon paper GDL and microporous layer may have played a positive role to protect the membrane from losing water to the dry cathode gas.

To summarize, quantification of species and current distributions in PEFCs, particularly under low-humidity conditions, is extremely desirable from the viewpoint of understanding and optimizing cell performance as well as providing valuable data for validation of computational fuel cell dynamics models.

Acknowledgments

Funding for this work from Nissan Motor Company Ltd. is gratefully acknowledged. The authors also thank Matthew Mench, G. Q. Lu, and Qunlong Dong of the Electrochemical Engine Center for their helpful discussions.

The Pennsylvania State University assisted in meeting the publication costs of this article.

List of Symbols

F	Faraday's constant, 96,487 C/equiv
I	current density, A/cm^2
n	molar flow rate, mol/s
P	pressure, atm
RH	relative humidity
x/L	fractional distance from the inlet

Greek

α	net water transport through the membrane from the anode to the cathode. H_2O/H^+
ξ	stoichiometry of reactant's supply

Superscripts

sat	saturation value

Subscripts

a	anode
c	cathode
H_2	hydrogen
in	inlet
O_2	oxygen
R	reaction
ref	reference condition
T	transport of water through the membrane
w	water
x	location of x/L

References

1. C. J. Brown, D. Pletcher, F. C. Walsh, J. K. Hammond, and D. Robinson, *J. Appl. Electrochem.*, **22**, 613 (1992).
2. S. J. C. Cleghorn, C. R. Derouin, M. S. Wilson, and S. Gottesfeld, *J. Appl. Electrochem.*, **28**, 663 (1998).
3. J. Stumper, S. Campell, D. Wilkinson, M. Johnson, and M. Davis, *Electrochim. Acta*, **43**, 3773 (1998).
4. Ch. Wiser, A. Helmbold, and E. Gue Lzow, *J. Appl. Electrochem.*, **30**, 803 (2000).
5. M. Noponen, T. Mennola, M. Mikkola, T. Hottinen, and P. Lund. *J. Power Sources*, **106**, 304 (2002).
6. D. J. L. Brett, S. Atkins, N. P. Brandon, V. Vesovic, N. Vasileiadis, and A. Kucernaka, *Electrochem. Solid-State Lett.*, **6**, A63 (2003).
7. M. M. Mench and C. Y. Wang, *J. Electrochem. Soc.*, **150**, A79 (2003).
8. M. M. Mench, C. Y. Wang, and M. Ishikawa, *J. Electrochem. Soc.*, **150**, A1052 (2003).
9. M. M. Mench, Q. L. Dong, and C. Y. Wang, *J. Power Sources*, **124**, 90 (2003).
10. C. Y. Wang, *Chem. Rev. (Washington, D.C.)*, **104**, 4727 (2004).
11. S. J. C. Cleghorn and J. A. Kolde, *2002 Fuel Cell Seminar*, Palm Springs, CA, Nov 2002.
12. H. A. Gasteiger, W. Gu, R. Makharia, M. F. Mathias, and B. Sompalli, *Handbook of Fuel Cells – Fundamentals, Technology and Applications*, Vol. 3, Wolf Vielstich, Hubert A. Gasteiger, and Arnold Lamm, Editors, p. 593, John Wiley & Sons, New York (2003).
13. Z. Ogumi, Z. Takehara, and S. Yoshizawa, *J. Electrochem. Soc.*, **131**, 769 (1984).
14. B. R. Breslau, and I. F. Miller, *Ind. Eng. Chem. Fundam.*, **10**, 554 (1971).
15. T. F. Fuller and J. Newman, *J. Electrochem. Soc.*, **139**, 1332 (1992).
16. T. A. Zawodzinski, Jr., J. Davey, J. Valerio, and S. Gottesfeld, *Electrochim. Acta*, **40**, 297 (1995).
17. G. J. M. Janssen and M. L. J. Overvelde, *J. Power Sources*, **101**, 117 (2001).